

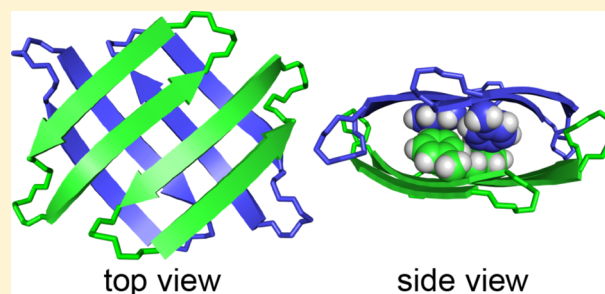
# A Tetramer Derived from Islet Amyloid Polypeptide

Yilin Wang, Adam G. Kreutzer, Nicholas L. Truex, and James S. Nowick\*<sup>1</sup>

Department of Chemistry, University of California, Irvine, Irvine, California 92697-2025, United States

## Supporting Information

**ABSTRACT:** Aggregation of the islet amyloid polypeptide (IAPP) to form fibrils and oligomers is important in the progression of type 2 diabetes. This article describes X-ray crystallographic and solution-state NMR studies of peptides derived from residues 11–17 of IAPP that assemble to form tetramers. Incorporation of residues 11–17 of IAPP (RLANFLV) into a macrocyclic  $\beta$ -sheet peptide results in a monomeric peptide that does not self-assemble to form oligomers. Mutation of Arg<sub>11</sub> to the uncharged isostere citrulline gives peptide homologues that assemble to form tetramers in both the crystal state and in aqueous solution. The tetramers consist of hydrogen-bonded dimers that sandwich together through hydrophobic interactions. The tetramers share several features with structures reported for IAPP fibrils and demonstrate the importance of hydrogen bonding and hydrophobic interactions in the oligomerization of IAPP-derived peptides.



The tetramers share several features with structures reported for IAPP fibrils and demonstrate the importance of hydrogen bonding and hydrophobic interactions in the oligomerization of IAPP-derived peptides.

## INTRODUCTION

Interactions among  $\beta$ -sheets are central to the misfolding and aggregation of peptides and proteins that form toxic oligomers and insoluble fibrils in over 40 amyloid diseases, including type 2 diabetes, Alzheimer's disease, and Parkinson's disease.<sup>1,2</sup> The fibrils share the common feature of an extended network of hydrogen-bonded  $\beta$ -sheets that are further stabilized through hydrophobic packing.<sup>3–11</sup> Less is known about the structures of the smaller, often metastable, and polymorphic oligomers, but  $\beta$ -sheets and hydrophobic interactions appear to be important in oligomer formation.<sup>12–17</sup>

The 37-residue islet amyloid polypeptide (IAPP) aggregates to form fibrils and oligomers that are central to islet  $\beta$ -cell death in the progression of type 2 diabetes.<sup>18–23</sup> Tycko and co-workers proposed structural models of IAPP fibrils using constraints from solid-state NMR spectroscopy.<sup>4</sup> In these models, a fibril consists of layers of parallel, in-register  $\beta$ -sheets that run perpendicular to the length of the fibril.  $\beta$ -Strands consisting of central residues 8–17 form one of the layers, while  $\beta$ -strands comprising C-terminal residues 28–36 form the other layer. A loop region containing residues 18–27 connects the two  $\beta$ -strands. Using X-ray crystallographic structures derived from fragments of IAPP, Eisenberg and co-workers constructed a similar fibril model in which the side chains are more tightly packed.<sup>5,24</sup> Langen and co-workers proposed a model of IAPP fibrils using constraints from EPR spectroscopy in which the  $\beta$ -strands pack more loosely.<sup>25</sup> The residues involved in  $\beta$ -sheet formation vary slightly among these different models, but central residues 12–17 and C-terminal residues 31–36 are generally thought to be involved in  $\beta$ -strand formation.

Although the structures of IAPP oligomers are not known at high resolution, they appear to be composed of  $\beta$ -sheets. Through ion mobility-mass spectrometry (IM-MS) studies in

conjunction with replica exchange molecular dynamics (REMD), Bowers and co-workers proposed  $\beta$ -hairpin building blocks for human IAPP oligomers.<sup>26,27</sup> Hoyer and co-workers obtained an NMR-based structure of IAPP in a  $\beta$ -hairpin conformation bound to an affibody and suggested that this  $\beta$ -hairpin might be involved in IAPP aggregation.<sup>23</sup> The  $\beta$ -hairpin comprises residues 12–28; residues 12–18 and residues 22–28 form  $\beta$ -strands, while residues 19–21 form a turn. In a separate study, Zanni and co-workers used 2D IR spectroscopy to show that residues 23–27 have  $\beta$ -sheet structure in the oligomer but form a disordered loop in the fibril.<sup>28</sup>

Our laboratory recently introduced macrocyclic  $\beta$ -sheet peptides as a platform to explore the interactions among  $\beta$ -sheets in amyloidogenic peptides and proteins (Chart 1).<sup>28,29</sup> The macrocyclic  $\beta$ -sheet peptides contain a peptide strand and a template strand that are connected by two  $\delta$ -linked ornithine ( $\delta$ Orn) turn units.<sup>30,31</sup> The peptide strand contains a heptapeptide sequence derived from an amyloidogenic peptide or protein. The template strand contains four additional  $\alpha$ -amino acids and the unnatural amino acid Hao, which mimics a tripeptide  $\beta$ -strand, templates  $\beta$ -sheet formation, and blocks uncontrolled aggregation.<sup>32</sup> Our laboratory has used macrocyclic  $\beta$ -sheet peptides containing heptapeptide segments from the  $\beta$ -amyloid peptide A $\beta$ ,  $\beta_2$ -microglobulin, and  $\alpha$ -synuclein as inhibitors to control amyloid aggregation and reduce amyloid toxicity.<sup>29</sup> Recently, we used NMR spectroscopy to study the homotetramers and heterotetramers formed by macrocyclic  $\beta$ -sheet peptides containing residues 17–23 and 30–36 from A $\beta$ .<sup>33,34</sup>

Received: May 8, 2017

Published: June 29, 2017

Chart 1

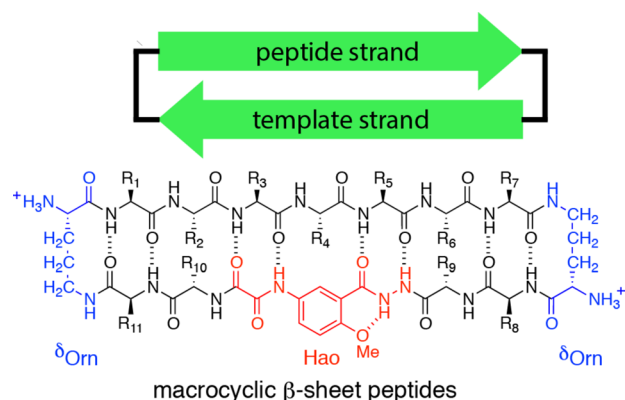
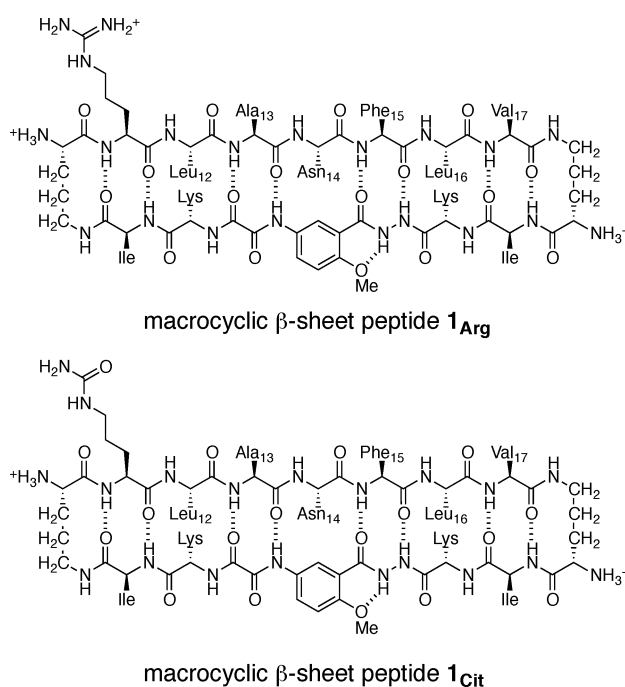


Chart 2



In the current study, we use macrocyclic  $\beta$ -sheet peptides as a platform to explore assembly of the central region of IAPP. We designed peptide **1Arg** to contain central residues 11–17 of IAPP (RLANFLV). We chose the IAPP<sub>11–17</sub> heptapeptide for its propensity to form a  $\beta$ -strand in fibrils and  $\beta$ -hairpin monomers. We also designed homologue peptide **1Cit** in which we mutated Arg<sub>11</sub> to the uncharged isostere of arginine, citrulline (Chart 2). Here we describe NMR spectroscopic studies of peptides **1Arg** and **1Cit**; report the X-ray crystallographic structure of a tetramer formed by a homologue of peptide **1Cit** and correlate the X-ray crystallographic structure with the solution-phase assembly of the IAPP-derived peptides.

## RESULTS

### Design and <sup>1</sup>H NMR Studies of Peptides **1Arg** and **1Cit**

The  $\beta$ -strand formed by IAPP<sub>11–17</sub> displays a hydrophobic surface comprising the side chains of Ala<sub>13</sub>, Phe<sub>15</sub>, and Val<sub>17</sub>, as well as Arg<sub>11</sub>. To reinforce the hydrophobicity of this surface, we incorporated isoleucine residues at positions R<sub>8</sub> and R<sub>11</sub> of the template strand. We incorporated lysine residues at positions R<sub>9</sub> and R<sub>10</sub> to increase solubility of the peptide and render the surface displaying the side chains of Leu<sub>12</sub>, Asn<sub>14</sub>, and Leu<sub>16</sub> hydrophilic.

In aqueous solution, peptide **1Arg** is monomeric. The <sup>1</sup>H NMR spectrum of peptide **1Arg** at 4 mM exhibits a single set of sharp resonances, associated with the monomeric peptide (Figure 1). The resonances associated with the  $\alpha$ -protons are in the 4–5 ppm range, showing little to no downfield shifting relative to the typical values for the corresponding residues in a random coil conformation (Figure S3).<sup>35</sup> At 8 mM, we observe broadening of the resonances but no additional peaks associated with assembly of the peptide (Figure S1). We hypothesized that the positive charge on Arg<sub>11</sub> may prevent peptide **1Arg** from oligomerizing. To explore this hypothesis, we replaced Arg<sub>11</sub> with the neutrally charged isostere citrulline, reducing the net charge from +5 to +4.

Peptide **1Cit** is monomeric at low concentrations but forms a tetramer at higher concentrations. At 1 mM, the spectrum is similar to that of peptide **1Arg** (Figures 1 and S2). At 4 mM, peptide **1Cit** displays two sets of broad resonances associated with the monomer and the tetramer. At 16 mM, only the resonances associated with the tetramer are visible. The resonances associated with the  $\alpha$ -protons of the tetramer are shifted downfield by up to 1 ppm relative to those of random coil

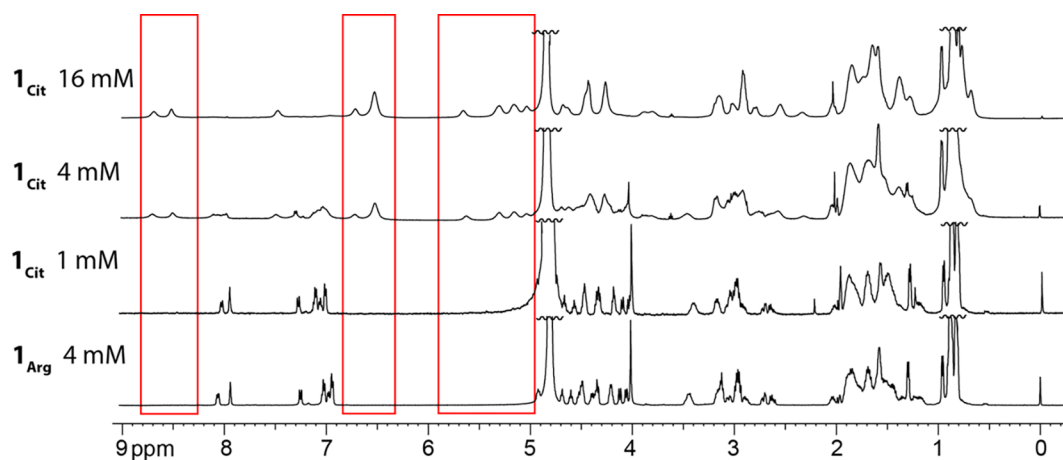


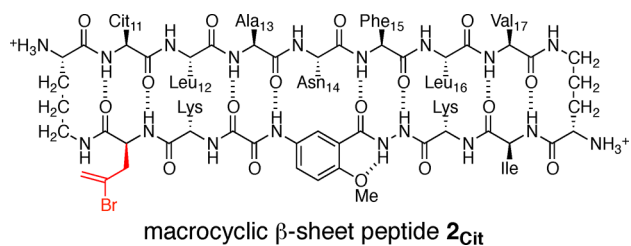
**Figure 1.** <sup>1</sup>H NMR spectra of macrocyclic  $\beta$ -sheet peptides **1Arg** and **1Cit** in 50 mM CD<sub>3</sub>COOD and 50 mM CD<sub>3</sub>COONa buffer in D<sub>2</sub>O at 298 K. The red boxes highlight noteworthy resonances of the tetramer.

values (Figure S4).<sup>35</sup> This downfield shifting reflects the folding and assembly of the peptide into the tetramer. The aromatic resonances associated with the Phe<sub>15</sub> side chain are shifted upfield by approximately 0.5 ppm, to 6.5 ppm, suggesting that the side chains of Phe<sub>15</sub> pack to form a hydrophobic core within the tetramer.

Comparison of <sup>1</sup>H NMR spectra of peptide **1**<sub>Cit</sub> at 1 mM and 16 mM shows that folding accompanies oligomerization. The magnetic anisotropy of the diastereotopic  $\delta$ -protons of the  $\delta$ Orn turn units reflects  $\beta$ -sheet folding in macrocyclic  $\beta$ -sheet peptides.<sup>30,31</sup> In a well-folded macrocyclic  $\beta$ -sheet peptide, each diastereotopic *pro-S*  $\delta$ -proton resonance is about 0.6 ppm downfield of the corresponding *pro-R*  $\delta$ -proton resonance. The monomer subunits of the tetramer formed by peptide **1**<sub>Cit</sub> are well folded, with the difference in chemical shifts of the diastereotopic *pro-S* and *pro-R*  $\delta$ -protons being 0.66 and 0.70 ppm. In contrast, monomeric peptide **1**<sub>Cit</sub> is partially folded, with the difference in chemical shifts of the diastereotopic *pro-S* and *pro-R*  $\delta$ -protons being 0.19 and 0.29 ppm.

**X-ray Crystallographic Structure of a Tetramer Derived from IAPP<sub>11–17</sub>.** To further characterize the structure of the tetramer formed by peptide **1**<sub>Cit</sub>, we turned to X-ray crystallography. To facilitate X-ray crystallographic phase determination, we designed and synthesized homologue peptide **2**<sub>Cit</sub> (Chart 3). Peptide **2**<sub>Cit</sub> contains the leucine isostere, (2-

Chart 3



bromoallyl)glycine, in place of one of the isoleucines in the template strand to allow X-ray crystallographic phase determination by means of single-wavelength anomalous diffraction phasing.<sup>13</sup> Peptide **2**<sub>Cit</sub> afforded crystals suitable for X-ray diffraction in conditions containing sodium citrate buffer, isopropanol, and poly(ethylene glycol) (PEG) 4000.

The asymmetric unit contains four folded macrocyclic  $\beta$ -sheets, which pack to form a tetramer. The heptapeptide  $\beta$ -strand of each monomer subunit is hydrogen bonded to the template strand through a network of eight hydrogen bonds (Figure 2A). The monomers in the asymmetric unit are similar in conformation with little variation in the side chains. One notable difference is in the Phe<sub>15</sub> residues, which exhibit two rotamers (Figure 2B).

The monomer subunits pair through edge-to-edge hydrogen bonding to form antiparallel  $\beta$ -sheet dimers (Figure 3). The two heptapeptide  $\beta$ -strands in the dimer are shifted by two residues toward the C-termini. Six intermolecular hydrogen bonds form between the two monomers. The dimer presents two surfaces. One surface is hydrophobic and displays the side chains of Cit<sub>11</sub>, Ala<sub>13</sub>, Phe<sub>15</sub>, and Val<sub>17</sub> of the peptide strand, as well as the Ile and (2-bromoallyl)glycine of the template strand (Figure 3A). The two Phe<sub>15</sub> side chains on the hydrophobic surface adopt different rotamers. The other surface is hydrophilic and displays the Leu<sub>12</sub>, Asn<sub>14</sub>, and Leu<sub>16</sub> side chains of the peptide strand, as well as the two Lys residues of the template strand (Figure 3B).

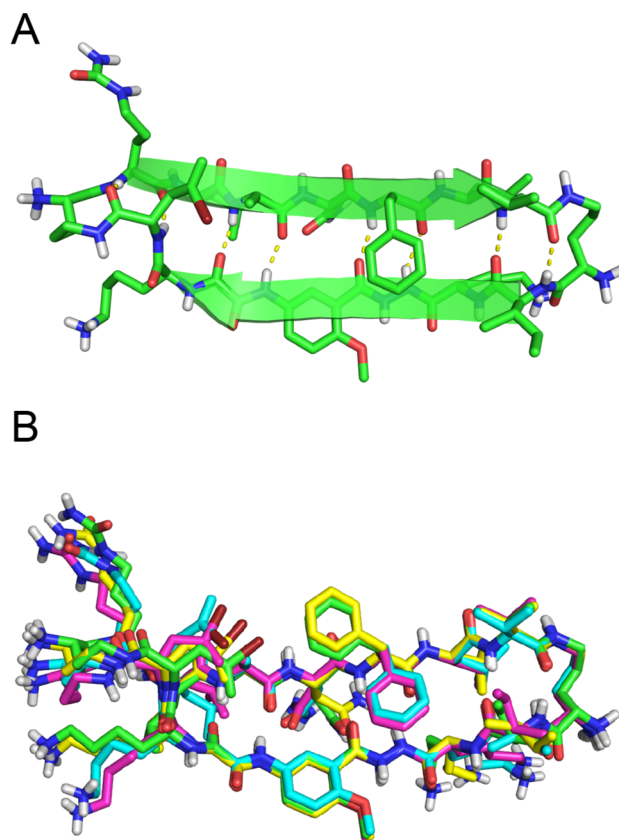


**Figure 2.** X-ray crystallographic structure of peptide **2**<sub>Cit</sub> (PDB SUHR). (A) Representative monomer subunit. (B) Overlay of the four monomers in the asymmetric unit.

Two hydrogen-bonded dimers sandwich together on their hydrophobic surfaces to form a tetramer (Figure 4). In the tetramer, the  $\beta$ -sheets of the dimers are nearly orthogonal. The side chains of Ala<sub>13</sub>, Phe<sub>15</sub>, Val<sub>17</sub>, Ile, and (2-bromoallyl)glycine create a hydrophobic core within the sandwich, with the four phenyl groups packing at the center of the sandwich. The two rotamers of the Phe<sub>15</sub> side chains allow the phenyl groups to pack together tightly through hydrophobic interactions and aromatic stacking at the center of the hydrophobic core. The side chains of Ala<sub>13</sub>, Val<sub>17</sub>, Ile, and (2-bromoallyl)glycine surround the four Phe<sub>15</sub> side chains, packing through hydrophobic interaction to stabilize the tetramer. The hydrophilic side chain of Cit<sub>11</sub> extends out of the hydrophobic core. The hydrophilic surfaces of the dimer subunits that comprise the tetramer are exposed to solvent.

**Solution-State Studies of a Tetramer Derived from IAPP<sub>11–17</sub>.** Diffusion-ordered spectroscopy (DOSY) provides a useful tool for assessing the relative oligomerization state of macrocyclic  $\beta$ -sheets peptides.<sup>33,34,36,37</sup> Oligomers diffuse more slowly than the monomers, with dimers having a diffusion coefficient of about 0.75–0.79 times that of the monomer and tetramers having a diffusion coefficient of about 0.58–0.63 times that of the monomer.<sup>33,37,38</sup> At 298 K, the diffusion coefficient of peptide **1**<sub>Arg</sub> is  $19.6 \times 10^{-7} \text{ cm}^2/\text{s}$  in deuterioacetate buffered D<sub>2</sub>O (Table 1). At 1 mM, peptide **1**<sub>Cit</sub> is monomeric, with a diffusion coefficient of  $20.0 \times 10^{-7} \text{ cm}^2/\text{s}$ , which is the same as peptide **1**<sub>Arg</sub> within the limits of experimental error. At 2 mM, peptide **1**<sub>Cit</sub> is largely monomeric, with a diffusion coefficient of  $18.9 \times 10^{-7} \text{ cm}^2/\text{s}$ .



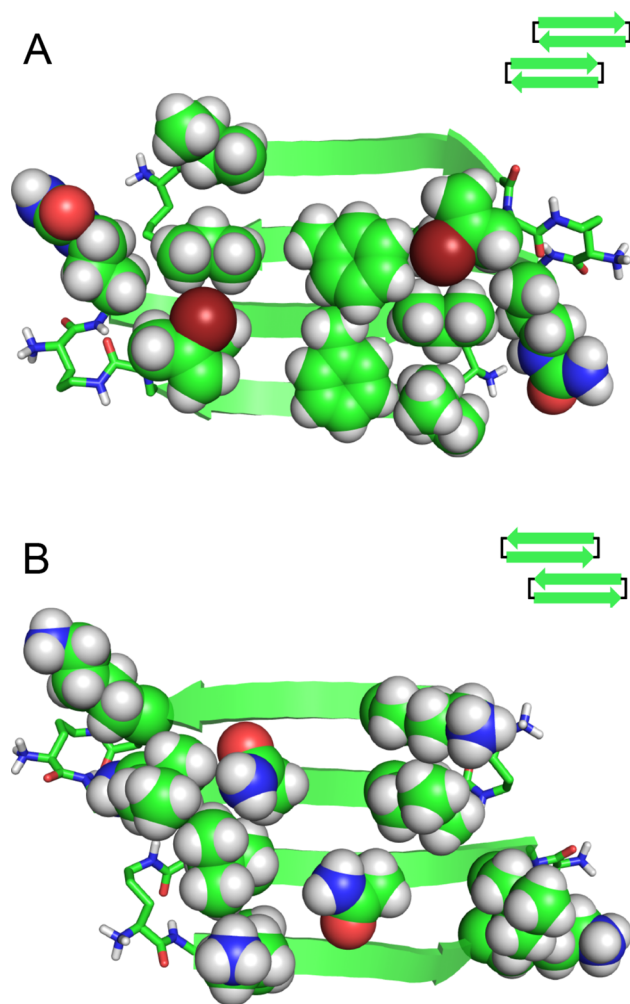


**Figure 3.** X-ray crystallographic structure of the dimer formed by peptide  $2_{\text{Cit}}$ . (A) View of the hydrophobic surface with side chains shown as spheres. (B) View of the hydrophilic surface with side chains shown as spheres.

As the concentration is increased and the resonances from the oligomer grow in, the diffusion coefficient of peptide  $1_{\text{Cit}}$  decreases. At 4 mM and 8 mM, discrete diffusion coefficients cannot be measured for the resonances associated with the monomer and the oligomer, because exchange occurs at a rate similar to the 75 ms time scale of the experiment. Instead, an averaged diffusion coefficient for the mixture is observed. At 4 mM, the diffusion coefficient is  $17.4 \times 10^{-7} \text{ cm}^2/\text{s}$ , and at 8 mM the diffusion coefficient is  $14.2 \times 10^{-7} \text{ cm}^2/\text{s}$ . At 16 mM, the oligomer predominates vastly, and only resonances for the oligomer are observed. At 16 mM, the diffusion coefficient is  $12.4 \times 10^{-7} \text{ cm}^2/\text{s}$ . This value is about 0.6 times that of the monomer of peptide  $1_{\text{Cit}}$ , and is consistent with a tetramer.

NOESY NMR spectroscopy establishes that the structure of the tetramer formed by peptide  $1_{\text{Cit}}$  in aqueous solution is similar to the tetramer observed for peptide  $2_{\text{Cit}}$  in the crystal. We observe NOEs from the folding of the monomers and formation of the dimers. Two strong crosspeaks in the NOESY spectrum reflect folding of macrocyclic  $\beta$ -sheet peptide  $1_{\text{Cit}}$ , one between the  $\alpha$ -protons of Leu and Lys, and one between the  $\alpha$ -proton of Asn<sub>14</sub> and the proton at the 6-position of the unnatural amino acid Hao (Figure 5). NOEs between the  $\alpha$ -proton and *pro-S*  $\delta$ -proton of the  $\delta^{\text{Orn}}$  turn units further reflect folding of the

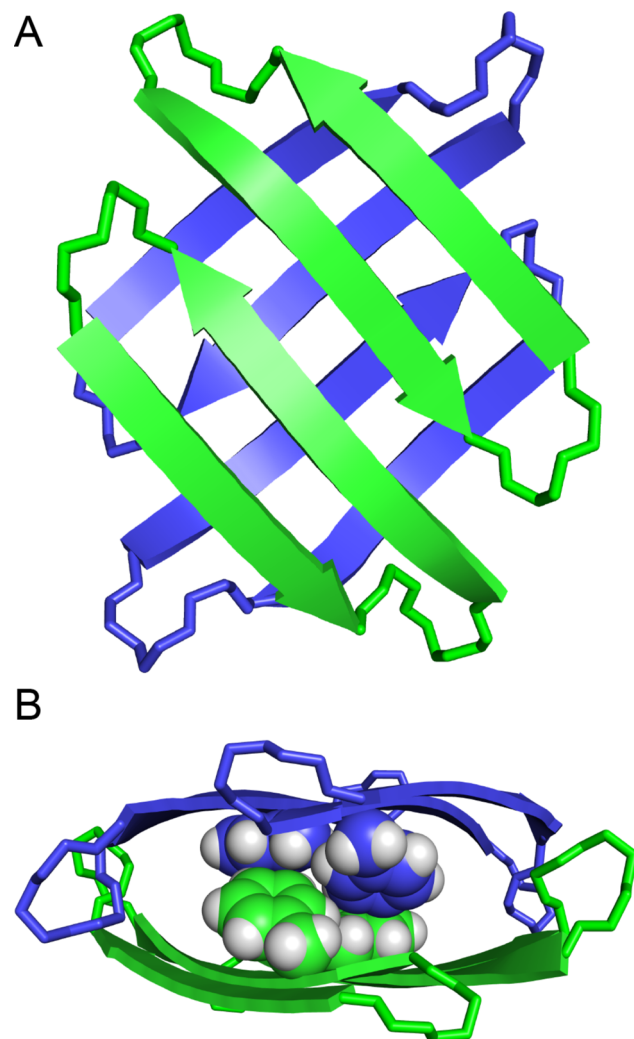


**Figure 4.** X-ray crystallographic structure of the tetramer of peptide  $2_{\text{Cit}}$ . (A) Top view. (B) Side view. Sphere representations of Phe<sub>15</sub> show packing of the aromatic side chains in the hydrophobic core.

**Table 1.** Diffusion Coefficients ( $D$ ) of Peptides  $1_{\text{Arg}}$  and  $1_{\text{Cit}}$  in 50 mM  $\text{CD}_3\text{COOD}$  and 50 mM  $\text{CD}_3\text{COONa}$  Buffer in  $\text{D}_2\text{O}$  at 298 K

	MW <sub>monomer</sub> (Da)	MW <sub>tetramer</sub> (Da)	conc. (mM)	$D$ ( $\times 10^{-7}$ $\text{cm}^2/\text{s}$ )	oligomer state
$1_{\text{Arg}}$	1759	7036	4	$19.6 \pm 0.6$	monomer
$1_{\text{Cit}}$	1760	7040	1	$20.0 \pm 2.0$	monomer
$1_{\text{Cit}}$	1760	7040	2	$18.9 \pm 1.2$	monomer
$1_{\text{Cit}}$	1760	7040	4	$17.4 \pm 1.2$	mixture
$1_{\text{Cit}}$	1760	7040	8	$14.2 \pm 0.3$	mixture
$1_{\text{Cit}}$	1760	7040	16	$12.4 \pm 0.3$	tetramer

macrocyclic. A strong crosspeak between the  $\alpha$ -protons of Ala<sub>13</sub> and Val<sub>17</sub> reflect shifted antiparallel dimer formation. An additional NOE between the methoxy protons of Hao and the Ile side chain reflect packing of the dimers in a sandwich-like fashion (Figure 6). The interlayer NOE between the Hao-methoxy and Ile side chain is characteristic of sandwich-like tetramers of Hao-containing macrocyclic  $\beta$ -sheet peptides.<sup>33</sup> These NOEs associated with folding, dimerization, and packing reflect the congruence of the X-ray crystallographic and solution-state tetramers.

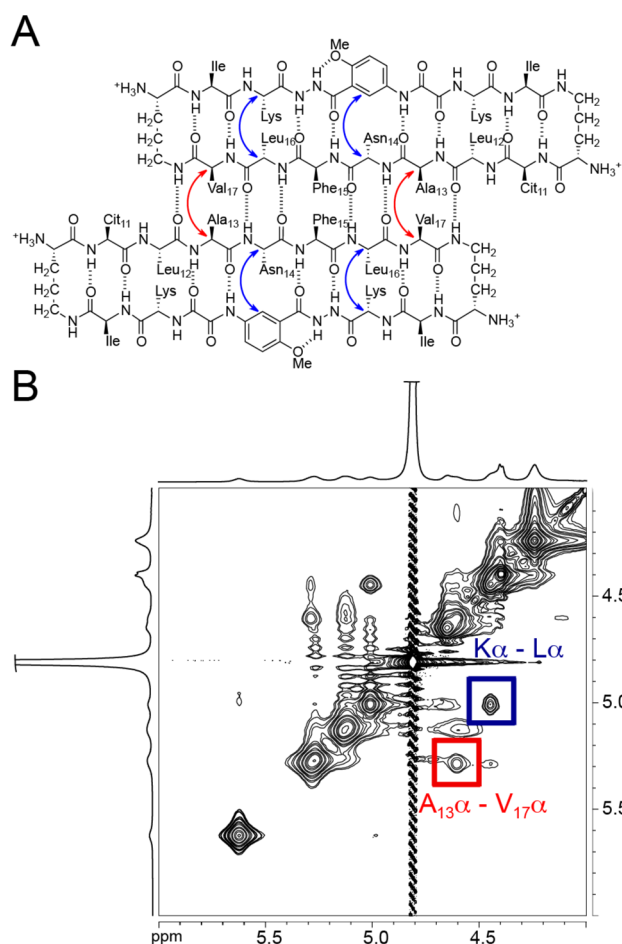


**Figure 5.** NOEs associated with the dimer subunit of peptide  $1_{\text{Cit}}$ . (A) Shifted, antiparallel hydrogen-bonded dimer. Blue arrows indicate intramolecular NOEs and red arrows indicate intermolecular NOE observed in the NOESY spectrum. (B) Expansion of the NOESY spectrum showing selected intramolecular (blue) and intermolecular (red) NOE crosspeaks.

## DISCUSSION

To understand why peptide  $1_{\text{Cit}}$  forms tetramers but peptide  $1_{\text{Arg}}$  does not, we used the X-ray crystallographic structure of peptide  $2_{\text{Cit}}$  to generate molecular models of tetramers of peptides  $1_{\text{Cit}}$  and  $1_{\text{Arg}}$ . We modeled the tetramer formed by peptide  $1_{\text{Cit}}$  by mutating the (2-bromoallyl)glycine residue to isoleucine and minimizing the resulting structure in MacroModel with the MMFFs force field with GB/SA water solvation (Figure S5). We modeled a tetramer of peptide  $1_{\text{Arg}}$  in a similar fashion, mutating both the (2-bromoallyl)glycine and the citrulline residues. Both molecular models overlay well with the X-ray crystallographic structure of the tetramer of peptide  $2_{\text{Cit}}$  (RMSD  $\sim 1$  Å). Inspection of the dimer subunits suggests an explanation of the differing stabilities of the  $1_{\text{Cit}}$  and  $1_{\text{Arg}}$  tetramers (Figure 7). In the dimer subunit of peptide  $1_{\text{Arg}}$ , the cationic guanidinium group of each arginine is near the ammonium group of one of the  $^{\text{o}}\text{Orn}$  turn units, while in the dimer subunit of peptide  $1_{\text{Cit}}$  the neutral urea group of citrulline is near the ammonium group. Thus, it appears that charge–charge repulsion destabilizes the dimer and hence the tetramer of peptide  $1_{\text{Arg}}$ .

The X-ray crystallographic structure and molecular model of the tetramers formed by peptides  $2_{\text{Cit}}$  and  $1_{\text{Cit}}$  share several features with structures reported for IAPP fibrils. Like the

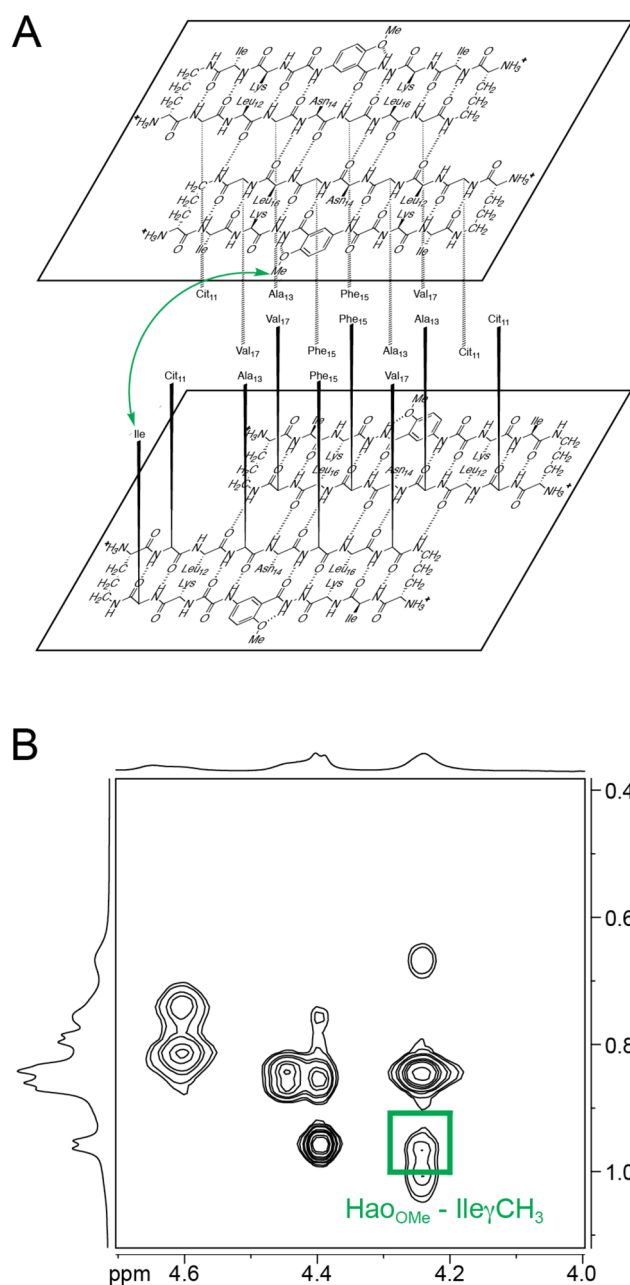


**Figure 6.** NOE associated with the tetramer of peptide  $1_{\text{Cit}}$ . (A) Green arrow indicates interlayer NOE observed in the NOESY spectrum. (B) NOE crosspeak between the Ile side chain and the methoxy protons of the unnatural amino acid Hao.

tetramers, the full atomic models of IAPP described by Tycko and co-workers consist of layered  $\beta$ -sheets in which hydrophobic interactions stabilize the layered structure. In contrast to the tetramers of peptides  $2_{\text{Cit}}$  and  $1_{\text{Cit}}$ , the fibrils consist of parallel  $\beta$ -sheets formed by IAPP rather than antiparallel  $\beta$ -sheets. In the two different fibril models proposed by Tycko and co-workers, the Phe<sub>15</sub> side chains are on either the interior or the exterior of the layers. The fragment-based model of IAPP fibrils proposed by Eisenberg and co-workers also consists of layered parallel  $\beta$ -sheets, with the side chains of Phe<sub>15</sub> on the exterior of the layers. Recently, Eisenberg and co-workers reported that IAPP<sub>15–25</sub> forms fibrils consisting of loosely laminated antiparallel  $\beta$ -sheets.<sup>39</sup> Hydrophobic interactions of Phe<sub>15</sub> appear to be more important in the NMR structure of the IAPP  $\beta$ -hairpin bound to

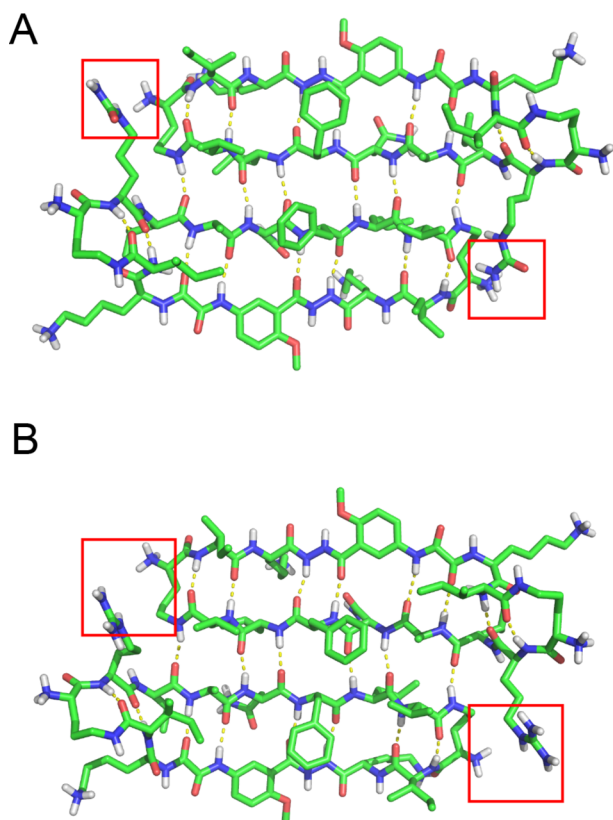
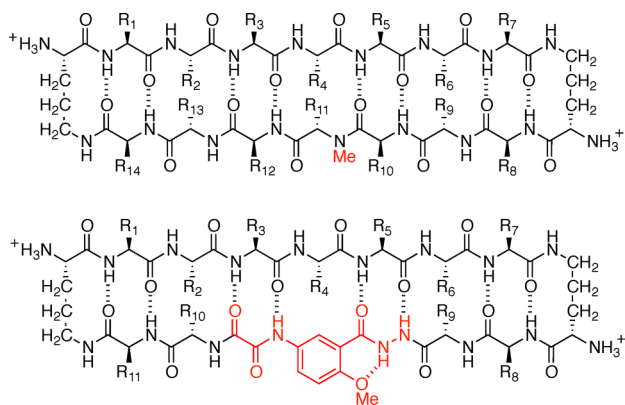


**Figure 7.** Crystallographically based molecular models of the dimer subunits of the tetramers of peptide **1<sub>Cit</sub>** (A) and **1<sub>Arg</sub>** (B). The red boxes highlight interactions between the ammonium groups of the  $\delta$ Orn turn units and the Arg<sub>11</sub> or Cit<sub>11</sub> side chains.

**Chart 4**



an affibody reported by Hoyer et al., in which the Phe<sub>15</sub> and Phe<sub>23</sub> pack tightly against one of the phenylalanine residues in the affibody to form a central core.<sup>23</sup> This mode of assembly is similar to the packing of Phe<sub>15</sub> in the tetramers formed by peptides **1<sub>Cit</sub>** and **2<sub>Cit</sub>**.

The tetramers formed by peptides **1<sub>Cit</sub>** and **2<sub>Cit</sub>** share common features with assemblies formed by other Hao-containing macrocyclic  $\beta$ -sheet peptides that our laboratory has studied (Chart 4). Several Hao-containing macrocyclic  $\beta$ -sheet peptides containing heptapeptide sequences from various amyloidogenic peptides and proteins form hydrogen-bonded assemblies laminated through hydrophobic interactions in the crystal state.<sup>29,40</sup> We have also identified two Hao-containing macro-

cyclic  $\beta$ -sheet peptides containing heptapeptide sequences from the  $\beta$ -amyloid peptide A $\beta$ , which assemble to form tetramers in solution.<sup>33,34</sup> The flat, hydrophobic Hao group appears to facilitate the formation of these layered structures.

These structures differ from those that we have observed for *N*-methylated macrocyclic  $\beta$ -sheet peptides, which we have also studied (Chart 4). Most of the *N*-methylated macrocyclic  $\beta$ -sheet peptides containing sequences from various amyloidogenic peptides and proteins that we have observed in the crystal state form compact higher-order oligomers, such as hexamers, octamers, nonamers, and dodecamers.<sup>15,16,41,42</sup> The *N*-methylated macrocyclic  $\beta$ -sheet peptides are generally more twisted than the Hao-containing macrocyclic  $\beta$ -sheet peptides. This twisting appears to facilitate assembly through interactions between curved hydrophobic surfaces, in addition to hydrogen bonding. The flat sandwich-like structures formed by the Hao-containing macrocyclic  $\beta$ -sheets resemble the laminated structures of amyloid fibrils, while the compact globular structures formed by the *N*-methylated macrocyclic  $\beta$ -sheets might offer a glimpse into the structures of amyloid oligomers.

## CONCLUSION

The <sup>1</sup>H NMR, X-ray crystallographic, and molecular modeling studies of peptides **1<sub>Arg</sub>**, **1<sub>Cit</sub>**, and **2<sub>Cit</sub>** described above demonstrate the importance of hydrogen bonding and hydrophobic interactions in the oligomerization of IAPP-derived peptides. Peptide **1<sub>Arg</sub>** remains monomeric in aqueous solution, whereas peptides **1<sub>Cit</sub>** and **2<sub>Cit</sub>** assemble to form tetramers in aqueous solution and in the crystal state. The differences between peptides **1<sub>Arg</sub>** and **1<sub>Cit</sub>** suggest that charge–charge interactions can modulate oligomer formation.

Our laboratory has previously used NMR spectroscopy and X-ray crystallography as complementary techniques to investigate the assembly of different macrocyclic  $\beta$ -sheet peptides derived from A $\beta$ .<sup>37,43</sup> In these studies, the macrocyclic  $\beta$ -sheet peptides assembled to form tetramers both in solution and in the crystal, but the structure of the tetramer formed in solution differed from the structure formed in the crystal. The findings of the current article are significant because they demonstrate that macrocyclic  $\beta$ -sheet peptides can assemble to form the same structure in solution and in the crystal state. Furthermore, the tetramer described here might serve as a structural model for understanding important contacts within oligomers and fibrils formed by full-length IAPP.

## EXPERIMENTAL SECTION

**Synthesis of Macrocyclic  $\beta$ -Sheet Peptides.** Synthesis and purification of the macrocyclic  $\beta$ -sheet peptides were performed as previously described.<sup>33</sup> The peptides were purified by reverse-phase HPLC and the pure fractions were lyophilized to give 22 mg of peptide **1<sub>Arg</sub>**, 37 mg of peptide **1<sub>Cit</sub>**, and 19 mg of **2<sub>Cit</sub>**. Based on resin loading, the yields are 9, 14, and 7%, respectively.

**Macrocyclic  $\beta$ -Sheet Peptide **1<sub>Arg</sub>**.** <sup>1</sup>H NMR, (500 MHz, 4 mM in D<sub>2</sub>O, 298 K)  $\delta$  8.06 (d, *J* = 8.6 Hz, 1H), 7.94 (s, 1H), 7.25 (d, *J* = 9.1 Hz, 1H), 6.92–7.05 (m, 5H), 4.92 (t, *J* = 7.2 Hz, 1H), 4.69 (t, *J* = 6.7 Hz, 1H), 4.60 (t, *J* = 7.1 Hz, 1H), 4.46–4.55 (m, 3H), 4.32–4.42 (m, 3H), 4.21 (m, 2H), 4.12 (d, *J* = 9.3 Hz, 1H), 4.06 (d, *J* = 8.7 Hz, 1H), 4.02 (s, 3H), 3.38–3.50 (m, 2H), 3.09–3.20 (m, 4H), 3.05 (dd, *J* = 14.2, 5.5 Hz, 1H), 2.92–3.02 (m, 4H), 2.88 (dd, *J* = 14.0, 6.6 Hz, 1H), 2.71 (dd, *J* = 15.3, 5.4 Hz, 1H), 2.62 (dd, *J* = 15.4, 8.8 Hz, 1H), 1.11–2.10 (m, 37H), 1.31 (d, *J* = 6.8 Hz, 3H), 0.96 (d, *J* = 6.4 Hz, 3H), 0.79–0.92 (m, 27H); HRMS (ESI-TOF) *m/z*: [M+H]<sup>+</sup> Calcd for C<sub>83</sub>H<sub>139</sub>N<sub>24</sub>O<sub>18</sub> 1760.0699; Found 1760.0710.



**Macrocyclic  $\beta$ -Sheet Peptide  $1_{\text{Cit}}$ .**  $^1\text{H}$  NMR, (500 MHz, 1 mM in  $\text{D}_2\text{O}$ , 298 K)  $\delta$  7.99 (d,  $J$  = 8.9 Hz, 1H), 7.91 (s, 1H), 7.25 (d,  $J$  = 9.2 Hz, 1H), 6.96–7.12 (m, 5H), 4.65 (t,  $J$  = 6.0 Hz, 1H), 4.56 (t,  $J$  = 7.3 Hz, 1H), 4.42–4.50 (m, 3H), 4.28–4.38 (m, 3H), 4.17 (t,  $J$  = 6.2 Hz, 2H), 4.09 (d,  $J$  = 8.3 Hz, 1H), 4.03 (d,  $J$  = 8.3 Hz, 1H), 4.00 (s, 3H), 3.33–3.44 (m, 2H), 3.12–3.21 (m, 2H), 2.88–3.10 (m, 8H), 2.71 (dd,  $J$  = 14.9, 5.5 Hz, 1H), 2.63 (dd,  $J$  = 15.7, 8.5 Hz, 1H), 1.35–2.07 (m, 35H), 1.28 (d,  $J$  = 7.1 Hz, 3H), 1.11–1.25 (m, 2H), 0.96 (d,  $J$  = 6.5 Hz, 3H), 0.78–0.93 (m, 27H); HRMS (ESI-TOF)  $m/z$ :  $[\text{M}+\text{Na}]^+$  Calcd for  $\text{C}_{83}\text{H}_{137}\text{N}_{23}\text{O}_{19}\text{Na}$  1783.0359; Found 1783.0337.

**Macrocyclic  $\beta$ -Sheet Peptide  $2_{\text{Cit}}$ .**  $^1\text{H}$  NMR, (500 MHz, 1 mM in  $\text{D}_2\text{O}$ , 298 K)  $\delta$  7.96 (d,  $J$  = 2.7 Hz, 1H), 7.90 (dd,  $J$  = 8.9, 2.6 Hz, 1H), 7.24 (d,  $J$  = 9.2 Hz, 1H), 7.02–7.16 (m, 5H), 5.77 (s, 1H), 5.57 (s, 1H), 4.69 (t,  $J$  = 6.5 Hz, 1H), 4.62–4.66 (m,  $J$  = 2H), 4.32–4.50 (m, 5H), 4.22–4.30 (m, 2H), 4.15 (t,  $J$  = 5.8 Hz, 1H), 4.10 (t,  $J$  = 5.7 Hz, 1H), 4.01 (d,  $J$  = 8.2 Hz, 1H), 3.98 (s, 3H), 3.25–3.37 (m, 1H), 3.20–3.26 (m, 1H), 3.13–3.20 (m, 1H), 3.00–3.10 (m, 3H), 2.99 (d,  $J$  = 7.4 Hz, 3H), 2.83–2.97 (m, 4H), 2.68 (qd,  $J$  = 6.1, 16 Hz, 1H), 1.40–2.05 (m, 34H), 1.24 (d,  $J$  = 6.8 Hz, 3H), 0.95 (d,  $J$  = 6.8 Hz, 3H), 0.80–0.91 (m, 21H). HRMS (ESI-TOF)  $m/z$ :  $[\text{M}+\text{H}]^+$  Calcd for  $\text{C}_{82}\text{H}_{132}\text{N}_{23}\text{O}_{19}\text{Br}$  1822.9331; Found 1822.9333.

**NMR Spectroscopy of the Macrocyclic  $\beta$ -Sheet Peptides.** **Sample Preparation.** NMR spectroscopy of the macrocyclic  $\beta$ -sheet peptides was performed in  $\text{D}_2\text{O}$  (D, 99.96%; Cambridge Isotope Laboratories, Inc.) with 50 mM  $\text{CD}_3\text{COOD}$  (D, 99.5%; Cambridge Isotope Laboratories, Inc.) and 50 mM  $\text{CD}_3\text{COONa}$  (D, 99%; Cambridge Isotope Laboratories, Inc.). The solutions were prepared by dissolving a weighed portion of the peptide in the appropriate volume of solvent. The molecular weights of the peptides were calculated as the TFA salts with all amino groups assumed to be protonated ( $1_{\text{Arg}}$ , M.W. 2330.24 mg/mL,  $1_{\text{Cit}}$ , M.W. 2331.24 mg/mL, and  $2_{\text{Cit}}$ , M.W. 2394.10 mg/mL). Each solution contained 4,4-dimethyl-4-silapentane-1-ammonium trifluoroacetate (DSA) as an internal standard for referencing chemical shifts.<sup>44</sup> The solutions were allowed to stand for 24 h to allow complete hydrogen to deuterium exchange of the amide NH protons.

**$^1\text{H}$  NMR, TOCSY, ROESY, and NOESY Data Collection.** NMR spectra were recorded on a Bruker 500 MHz spectrometer with a TCI cryoprobe. TOCSY spectra were recorded with 2048 points in the  $f_2$  dimension and 512 increments in the  $f_1$  dimension with a 150 ms spin-lock mixing time. TOCSY spectra were recorded with 2048 points in the  $f_2$  dimension and 512 increments in the  $f_1$  dimension with either a 100 or 150 ms spin-lock mixing time. NOESY spectra were recorded with 2048 points in the  $f_2$  dimension and 512 increments in the  $f_1$  dimension with a 150 ms mixing time.

**$^1\text{H}$  NMR, TOCSY, and NOESY Data Processing.** NMR spectra were processed with BrukerXwinNMR software. Automatic baseline correction was applied in both dimensions after phasing the spectra. TOCSY spectra were Fourier transformed to a final matrix size of 4096  $\times$  1024 real points using a Qsine weighting function and forward linear prediction. NOESY and ROESY spectra were Fourier transformed to a final matrix size of 4096  $\times$  2048 real points using a Qsine weighting function and forward linear prediction.

**Diffusion-Ordered Spectroscopy (DOSY) Experiments.** DOSY experiments were performed on a Bruker 500 MHz spectrometer equipped with a TCI cryoprobe, with a diffusion delay ( $\Delta$ ) of 75 ms and a diffusion gradient length ( $\delta$ ) of 2.5 ms. Sixteen sets of FIDs were recorded with the gradient strength incremented from 5–95% using a linear ramp. The combined FIDs were Fourier transformed in Bruker's TopSpin software to give a pseudo-2D spectrum. After phasing and performing baseline correction, each pseudo-2D spectrum was processed with logarithmic scaling on the Y-axis. The Y-axis was calibrated to the diffusion coefficient of the residual HOD peak in  $\text{D}_2\text{O}$  ( $1.9 \times 10^{-9} \text{ m}^2/\text{s}$  at 298 K).<sup>45</sup> The diffusion coefficients of the peptides were read and converted from logarithmic values to linear values.

**Crystallization of Peptide  $2_{\text{Cit}}$ .** The procedures in this section follow closely to those our laboratory has previously published.<sup>15</sup> Initial crystallization conditions for peptide  $2_{\text{Cit}}$  were determined using the hanging-drop vapor-diffusion method. Crystallization conditions were screened using three crystallization kits in a 96-well plate format (Hampton Index, PEG/Ion, and Crystal Screen). Three 150 nL hanging

drops that differed in the ratio of peptide to well solution were made per condition in each 96-well plate for a total of 864 experiments. Hanging drops were made by combining an appropriate volume of peptide  $2_{\text{Cit}}$  (10 mg/mL in deionized water) with an appropriate volume of well solution to create three 150-nL hanging drops with 1:1, 1:2, and 2:1 peptide:well solution. The hanging drops were made using a TTP LabTech Mosquito nanodisperse instrument. Crystals of peptide  $2_{\text{Cit}}$  grew in  $\sim 48$  h in a solution of 0.1 M sodium citrate at pH 5.0, 20% (v/v) isopropanol, and 18% PEG 4000.

Crystallization conditions for peptide  $2_{\text{Cit}}$  were optimized using a 4  $\times$  6 matrix Hampton VDX 24-well plate. The sodium citrate pH was varied in each row in increments of 0.5 pH units (4.0, 4.5, 5.0, and 5.5) and the isopropanol concentration in each column in increments of 2% (26, 24, 22, 20, 18, 16%). The first well in the 4  $\times$  6 matrix was prepared by combined 100  $\mu\text{L}$  of 1 M sodium citrate at pH 4.0, 260  $\mu\text{L}$  of isopropanol, 360  $\mu\text{L}$  of 50% (w/v) PEG 4000, and 280  $\mu\text{L}$  of deionized water. The other wells were prepared in analogous fashion, by combining 100  $\mu\text{L}$  of sodium citrate of varying pH, 360  $\mu\text{L}$  of 50% (w/v) PEG 4000, isopropanol in varying amounts, and deionized water for a total volume of 1 mL in each well.

Three hanging-drops were prepared per borosilicate glass slide by combining a solution of peptide  $2_{\text{Cit}}$  (10 mg/mL in deionized water) and the well solution in the following amounts: 1  $\mu\text{L}$ :1  $\mu\text{L}$ , 2  $\mu\text{L}$ :1  $\mu\text{L}$ , and 1  $\mu\text{L}$ :2  $\mu\text{L}$ . Slides were inverted and pressed firmly against the silicone grease surrounding each well. Crystals of peptide  $2_{\text{Cit}}$  suitable for X-ray diffraction grew in  $\sim 3$  days. Crystallization conditions were further optimized using smaller variations in sodium citrate pH (in increments of 0.2 pH units) and isopropanol concentrations (in increments of 1%). Crystals were harvested with a nylon loop attached to a copper or steel pin and flash frozen in liquid nitrogen prior to data collection. The optimized crystallization conditions for peptide  $2_{\text{Cit}}$  are summarized in Table S1.

**X-ray Crystallographic Data Collection, Data Processing, and Structure Determination for Peptide  $2_{\text{Cit}}$ .** Diffraction data for peptide  $2_{\text{Cit}}$  were collected at the Stanford Synchrotron Radiation Lightsource (SSRL) with a synchrotron source at 0.92-Å wavelength. Diffraction data were scaled and merged using XDS.<sup>46</sup> Coordinates for the anomalous signal were determined by HySS in the Phenix software suite 1.10.1.<sup>47</sup> The electron density map was generated in Phaser using the coordinates of the bromine anomalous signal. Molecular manipulation of the model was performed with Coot. Coordinates were refined with phenix.refine.

**Molecular Modeling of the Macrocyclic  $\beta$ -Sheet Peptides.** Molecular models of the tetramers of peptides  $1_{\text{Arg}}$  and  $1_{\text{Cit}}$  were generated from the X-ray crystallographic structure of the homologous peptide  $2_{\text{Cit}}$  (PDB: SUHR). We modeled the tetramer formed by peptides  $1_{\text{Cit}}$  by mutating the (2-bromoallyl)glycine residue to isoleucine and the side chain torsion angles were adjusted to match the resulting NOE. We modeled a tetramer of peptide  $1_{\text{Arg}}$  in a similar fashion, mutating both the (2-bromoallyl)glycine and the citrulline residues. The coordinates were exported from PyMOL and the file was imported into MacroModel with the Maestro user interface. Atom types and bond orders were edited as needed to correct errors in bond type and charge. Minimization was performed with the MMFFs force field and GB/SA water solvation.

## ■ ASSOCIATED CONTENT

### § Supporting Information

The Supporting Information is available free of charge on the ACS Publications website at DOI: 10.1021/acs.joc.7b01116.

X-ray crystallographic data of peptide  $2_{\text{Cit}}$  (CIF)

Supplementary figures and table; procedures for NMR spectroscopy and molecular modeling of macrocyclic  $\beta$ -sheet peptides; HPLC and MS characterization data for peptides  $1_{\text{Arg}}$ ,  $1_{\text{Cit}}$ , and  $2_{\text{Cit}}$  and NMR spectroscopic data for peptides (PDF)

Crystallographic coordinates of peptide  $2_{\text{Cit}}$  (SUHR) (PDB)

## ■ AUTHOR INFORMATION

## Corresponding Author

\*jsnowick@uci.edu

ORCID 

James S. Nowick: 0000-0002-2273-1029

## Notes

The authors declare no competing financial interest.

## ■ ACKNOWLEDGMENTS

We thank the National Science Foundation (NSF CHE-1507840) for funding and the Stanford Synchrotron Radiation Lightsource (SSRL) for synchrotron data collection. Use of the Stanford Synchrotron Radiation Lightsource, SLAC National Accelerator Laboratory, is supported by the U.S. Department of Energy, Office of Science, Office of Basic Energy Sciences under Contract No. DE-AC02-76SF00515. The SSRL Structural Molecular Biology Program is supported by the DOE Office of Biological and Environmental Research, and by the National Institutes of Health, National Institute of General Medical Sciences (including P41GM103393). The contents of this publication are solely the responsibility of the authors and do not necessarily represent the official views of NIGMS or NIH.

## ■ REFERENCES

- (1) Chiti, F.; Dobson, C. M. *Annu. Rev. Biochem.* **2006**, *75*, 333–366.
- (2) Knowles, T. P. J.; Vendruscolo, M.; Dobson, C. M. *Nat. Rev. Mol. Cell Biol.* **2014**, *15*, 384–396.
- (3) Nelson, R.; Sawaya, M. R.; Balbirnie, M.; Madsen, A. O.; Riekel, C.; Grothe, R.; Eisenberg, D. *Nature* **2005**, *435*, 773–778.
- (4) Luca, S.; Yau, W. M.; Leapman, R.; Tycko, R. *Biochemistry* **2007**, *46*, 13505–13522.
- (5) Wiltzius, J. J. W.; Sievers, S. A.; Sawaya, M. R.; Cascio, D.; Popov, D.; Riekel, C.; Eisenberg, D. *Protein Sci.* **2008**, *17*, 1467–1474.
- (6) Lu, J. X.; Qiang, W.; Yau, W. M.; Schwieters, C. D.; Meredith, S. C.; Tycko, R. *Cell* **2013**, *154*, 1257–1268.
- (7) Xiao, Y. L.; Ma, B. Y.; McElheny, D.; Parthasarathy, S.; Long, F.; Hoshi, M.; Nussinov, R.; Ishii, Y. *Nat. Struct. Mol. Biol.* **2015**, *22*, 499–505.
- (8) Lendel, C.; Bjerring, M.; Dubnovitsky, A.; Kelly, R. T.; Filippov, A.; Antzutkin, O. N.; Nielsen, N. C.; Hard, T. *Angew. Chem., Int. Ed.* **2014**, *53*, 12756–12760.
- (9) Xiao, Y. L.; Ma, B. Y.; McElheny, D.; Parthasarathy, S.; Long, F.; Hoshi, M.; Nussinov, R.; Ishii, Y. *Nat. Struct. Mol. Biol.* **2015**, *22*, 499–505.
- (10) Walti, M. A.; Ravotti, F.; Arai, H.; Glabe, C. G.; Wall, J. S.; Bockmann, A.; Guntert, P.; Meier, B. H.; Riek, R. *Proc. Natl. Acad. Sci. U. S. A.* **2016**, *113*, E4976–E4984.
- (11) Colvin, M. T.; Silvers, R.; Ni, Q. Z.; Can, T. V.; Sergeev, I.; Rosay, M.; Donovan, K. J.; Michael, B.; Wall, J.; Linse, S.; Griffin, R. G. *J. Am. Chem. Soc.* **2016**, *138*, 9663–9674.
- (12) Sandberg, A.; Luheshi, L. M.; Sollvander, S.; de Barros, T. P.; Macao, B.; Knowles, T. P. J.; Biverstal, H.; Lendel, C.; Ekholm-Petterson, F.; Dubnovitsky, A.; Lannfelt, L.; Dobson, C. M.; Hard, T. *Proc. Natl. Acad. Sci. U. S. A.* **2010**, *107*, 15595–15600.
- (13) Laganowsky, A.; Liu, C.; Sawaya, M. R.; Whitelegge, J. P.; Park, J.; Zhao, M. L.; Pensalfini, A.; Soriaga, A. B.; Landau, M.; Teng, P. K.; Cascio, D.; Glabe, C.; Eisenberg, D. *Science* **2012**, *335*, 1228–1231.
- (14) Mirecka, E. A.; Shaykhalishahi, H.; Gauhar, A.; Akgul, S.; Lecher, J.; Willbold, D.; Stoldt, M.; Hoyer, W. *Angew. Chem., Int. Ed.* **2014**, *53*, 4227–4230.
- (15) Spencer, R. K.; Kreutzer, A. G.; Salveson, P. J.; Li, H.; Nowick, J. S. *J. Am. Chem. Soc.* **2015**, *137*, 6304–6311.
- (16) Salveson, P. J.; Spencer, R. K.; Nowick, J. S. *J. Am. Chem. Soc.* **2016**, *138*, 4458–4467.
- (17) Kreutzer, A. G.; Hamza, I. L.; Spencer, R. K.; Nowick, J. S. *J. Am. Chem. Soc.* **2016**, *138*, 4634–4642.
- (18) Janson, J.; Ashley, R. H.; Harrison, D.; McIntyre, S.; Butler, P. C. *Diabetes* **1999**, *48*, 491–498.
- (19) Meier, J. J.; Kaye, R.; Lin, C. Y.; Gurlo, T.; Haataja, L.; Jayasinghe, S.; Langen, R.; Glabe, C. G.; Butler, P. C. *Am. J. Physiol. Endocrinol. Metab.* **2006**, *291*, E1317–E1324.
- (20) Konarkowska, B.; Aitken, J. F.; Kistler, J.; Zhang, S. P.; Cooper, G. J. S. *FEBS J.* **2006**, *273*, 3614–3624.
- (21) Westermark, P.; Andersson, A.; Westermark, G. T. *Physiol. Rev.* **2011**, *91*, 795–826.
- (22) Bram, Y.; Frydman-Marom, A.; Yanai, I.; Gilead, S.; Shaltiel-Karyo, R.; Amdursky, N.; Gazit, E. *Sci. Rep.* **2015**, *4*, 4267.
- (23) Mirecka, E. A.; Feuerstein, S.; Gremer, L.; Schroder, G. F.; Stoldt, M.; Willbold, D.; Hoyer, W. *Sci. Rep.* **2016**, *6*, 33474.
- (24) Soriaga, A. B.; Sangwan, S.; Macdonald, R.; Sawaya, M. R.; Eisenberg, D. *J. Phys. Chem. B* **2016**, *120*, 5810–5816.
- (25) Bedrood, S.; Li, Y. Y.; Isas, J. M.; Hegde, B. G.; Baxa, U.; Haworth, I. S.; Langen, R. *J. Biol. Chem.* **2012**, *287*, 5235–5241.
- (26) Dupuis, N. F.; Wu, C.; Shea, J. E.; Bowers, M. T. *J. Am. Chem. Soc.* **2009**, *131*, 18283–18292.
- (27) Dupuis, N. F.; Wu, C.; Shea, J. E.; Bowers, M. T. *J. Am. Chem. Soc.* **2011**, *133*, 7240–7243.
- (28) Buchanan, L. E.; Dunkelberger, E. B.; Tran, H. Q.; Cheng, P. N.; Chiu, C. C.; Cao, P.; Raleigh, D. P.; de Pablo, J. J.; Nowick, J. S.; Zanni, M. T. *Proc. Natl. Acad. Sci. U. S. A.* **2013**, *110*, 19285–19290.
- (29) Cheng, P. N.; Liu, C.; Zhao, M. L.; Eisenberg, D.; Nowick, J. S. *Nat. Chem.* **2012**, *4*, 927–933.
- (30) Nowick, J. S.; Lam, K. S.; Khasanova, T. V.; Kemnitzer, W. E.; Maitra, S.; Mee, H. T.; Liu, R. W. *J. Am. Chem. Soc.* **2002**, *124*, 4972–4973.
- (31) Nowick, J. S.; Brower, J. O. *J. Am. Chem. Soc.* **2003**, *125*, 876–877.
- (32) Nowick, J. S.; Chung, D. M.; Maitra, K.; Maitra, S.; Stigers, K. D.; Sun, Y. *J. Am. Chem. Soc.* **2000**, *122*, 7654–7661.
- (33) Truex, N. L.; Wang, Y. L.; Nowick, J. S. *J. Am. Chem. Soc.* **2016**, *138*, 13882–13890.
- (34) Truex, N. L.; Nowick, J. S. *J. Am. Chem. Soc.* **2016**, *138*, 13891–13900.
- (35) Wishart, D. S.; Sykes, B. D. *Methods Enzymol.* **1994**, *239*, 363–392.
- (36) Khakshoor, O.; Demeler, B.; Nowick, J. S. *J. Am. Chem. Soc.* **2007**, *129*, 5558–5569.
- (37) Pham, J. D.; Demeler, B.; Nowick, J. S. *J. Am. Chem. Soc.* **2014**, *136*, 5432–5442.
- (38) Polson, A. *J. Phys. Colloid Chem.* **1950**, *54*, 649–652.
- (39) Krotee, P.; Rodriguez, J. A.; Sawaya, M. R.; Cascio, D.; Reyes, F. E.; Shi, D.; Hattne, J.; Nannenga, B. L.; Oskarsson, M. E.; Philipp, S.; Griner, S.; Jiang, L.; Glabe, C. G.; Westermark, G. T.; Gonen, T.; Eisenberg, D. *eLife* **2017**, *6*, e19723.
- (40) Liu, C.; Zhao, M. L.; Jiang, L.; Cheng, P. N.; Park, J.; Sawaya, M. R.; Pensalfini, A.; Gou, D. W.; Berk, A. J.; Glabe, C. G.; Nowick, J.; Eisenberg, D. *Proc. Natl. Acad. Sci. U. S. A.* **2012**, *109*, 20913–20918.
- (41) Spencer, R. K.; Li, H.; Nowick, J. S. *J. Am. Chem. Soc.* **2014**, *136*, 5595–5598.
- (42) Yoo, S.; Kreutzer, A. G.; Truex, N. L.; Nowick, J. S. *Chem. Sci.* **2016**, *7*, 6946–6951.
- (43) Pham, J. D.; Chim, N.; Goulding, C. W.; Nowick, J. S. *J. Am. Chem. Soc.* **2013**, *135*, 12460–12467.
- (44) Nowick, J. S.; Khakshoor, O.; Hashemzadeh, M.; Brower, J. O. *Org. Lett.* **2003**, *5*, 3511–3513.
- (45) Longworth, L. G. *J. Phys. Chem.* **1960**, *64*, 1914–1917.
- (46) Kabsch, W. *Acta Crystallogr., Sect. D: Biol. Crystallogr.* **2010**, *66*, 125–132.
- (47) Adams, P. D.; Afonine, P. V.; Bunkoczi, G.; Chen, V. B.; Davis, I. W.; Echols, N.; Headd, J. J.; Hung, L. W.; Kapral, G. J.; Grosse-Kunstleve, R. W.; McCoy, A. J.; Moriarty, N. W.; Oeffner, R.; Read, R. J.; Richardson, D. C.; Richardson, J. S.; Terwilliger, T. C.; Zwart, P. H. *Acta Crystallogr., Sect. D: Biol. Crystallogr.* **2010**, *66*, 213–221.